



HAL
open science

A multidisciplinary study of a slow-slipping fault for seismic hazard assessment: The example of the Middle Durance Fault (SE France)

E.M. Cushing, O Bellier, S. Nechtschein, M. Sebrier, A. Lomax, P.H. Volant,
P. Dervin, P. Guignard, L. Bove

► To cite this version:

E.M. Cushing, O Bellier, S. Nechtschein, M. Sebrier, A. Lomax, et al.. A multidisciplinary study of a slow-slipping fault for seismic hazard assessment: The example of the Middle Durance Fault (SE France). *Geophysical Journal International*, 2008, 172 (3), pp.1163-1178. 10.1111/j.1365-246X.2007.03683.x . hal-03001426

HAL Id: hal-03001426

<https://hal.science/hal-03001426>

Submitted on 30 Sep 2021

HAL is a multi-disciplinary open access archive for the deposit and dissemination of scientific research documents, whether they are published or not. The documents may come from teaching and research institutions in France or abroad, or from public or private research centers.

L'archive ouverte pluridisciplinaire **HAL**, est destinée au dépôt et à la diffusion de documents scientifiques de niveau recherche, publiés ou non, émanant des établissements d'enseignement et de recherche français ou étrangers, des laboratoires publics ou privés.



Distributed under a Creative Commons Attribution 4.0 International License

A multidisciplinary study of a slow-slipping fault for seismic hazard assessment: the example of the Middle Durance Fault (SE France)

E. M. Cushing,¹ O. Bellier,² S. Nechtschein,¹ M. Sébrier,³ A. Lomax,⁴ Ph. Volant,¹ P. Dervin,¹ P. Guignard² and L. Bove⁵

¹IRSN, Institut de Radioprotection et de Sûreté Nucléaire, B.P. 17, F-92 262 Fontenay-aux-Roses Cedex, France

²CEREGE – UMR CNRS 6635 – Université Paul Cézanne Aix-Marseille 13545 Aix-en-Provence Cedex 4, France

³Université Pierre et Marie Curie – Paris VI Laboratoire de Tectonique – CNRS UMR 7072, F-75252 Paris Cedex 05, France

⁴A. Lomax Scientific, 161 Allee du Micocoulier, 06370 Mouans-Sartoux, France

⁵Toreador Energy SCS, 9 rue Scribe 75009 Paris, France

Accepted 2007 November 6. Received 2007 October 16; in original form 2006 December 19

SUMMARY

Assessing seismic hazard in continental interiors is difficult because these regions are characterized by low strain rates and may be struck by infrequent destructive earthquakes. In this paper, we provide an example showing that interpretations of seismic cross sections combined with other kinds of studies such as analysis of microseismicity allow the whole seismogenic source area to be imaged in this type of region. The Middle Durance Fault (MDF) is an 80-km-long fault system located southeastern France that has a moderate but regular seismicity and some palaeoseismic evidence for larger events. It behaves as an oblique ramp with a left-lateral-reverse fault slip and has a low strain rate. MDF is one of the rare slow active fault system monitored by a dedicated dense velocimetric short period network. This study showed a fault system segmented in map and cross section views which consists of staircase basement faults topped by listric faults ramping off Triassic evaporitic beds. Seismic sections allowed the construction of a 3-D structural model used for accurate location of microseismicity. Southern part of MDF is mainly active in the sedimentary cover. In its northern part and in Alpine foreland, seismicity deeper than 8 km was also recorded meaning active faults within the crust cannot be excluded. Seismogenic potential of MDF was roughly assessed. Resulting source sizes and estimated slip rates imply that the magnitude upper limit ranges from 6.0 to 6.5 with a return period of a few thousand years. The present study shows that the coupling between 3-D fault geometry imaging and accurate location of microseismicity provides a robust approach to analyse active fault sources and consequently a more refined seismic hazard assessment.

Key words: Palaeoseismology; Seismicity and tectonics; Continental neotectonics; Dynamics and mechanics of faulting; Europe.

1 INTRODUCTION

Although continental interiors are characterized by low strain rates, they can be struck by destructive earthquakes, for example, Bhuj (Bendick *et al.* 2001), Chirpan, (Vanneste *et al.* 2006), Struma (Meyer *et al.* 2007) and New Madrid (Tuttle *et al.* 2002). The direct consequence of these low strain rates is that recurrence intervals between destructive earthquakes are long, they can reach several millennia. In such regions, historical seismicity cannot document an entire earthquake cycle. Furthermore, erosion processes may not favour surface preservation of active fault traces. Therefore usual approaches developed for regions with high seismic activity, that is, historical seismicity investigations and palaeoseismology, are strongly limited and sometimes irrelevant for assessing seismic hazard in low strain rate areas.

Studies in the New Madrid region (Crone *et al.* 1985; Crone 1998; Chen *et al.* 2006) have shown that coupling accurate subsurface fault geometry with a detailed microseismicity is a robust tool to address dimensions of active faults. It then leads to better magnitude estimates for future seismic ruptures. In this paper, we provide a case study illustrating such coupling that allows a better assessment of active fault segmentation and consequently more refined estimates of seismic source characteristics for the Provence region in southeastern France.

Western Europe is characterized by weak to moderate seismic activity due to low NNW-trending convergence between Eurasian and African Plates ranging from 4 to 6 mm yr⁻¹ (DeMets *et al.* 1990, 1994; Argus *et al.* 1999). GPS data show that the convergence is mainly accommodated by deformation within a zone surrounded by Spain, Sardinia, Sicily and Northern Africa (Nocquet 2002). As

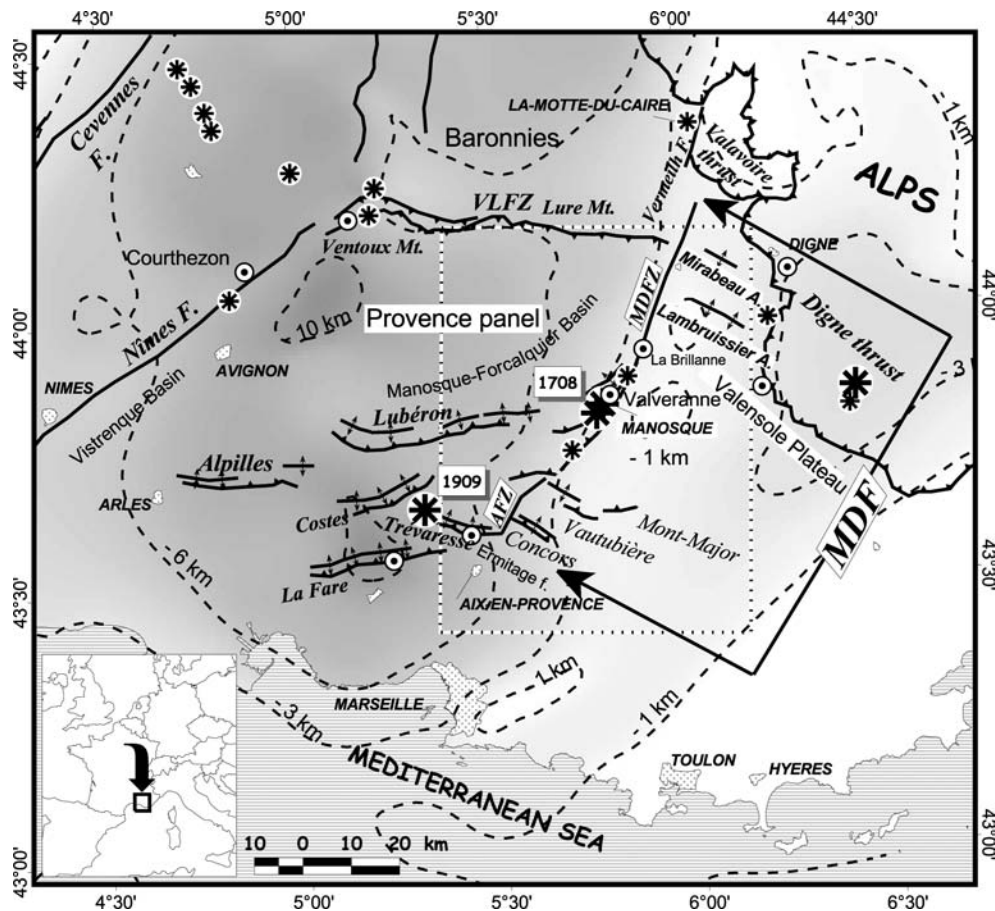


Figure 1. Main geological features of southeastern France: VLFZ = Ventoux-Lure Fault Zone, AFZ = Aix Fault Zone, MDFZ = Middle Durance Fault Zone. The Middle Durance Fault (MDF) consists of AFZ and MDFZ. Miocene to Quaternary fold axes are displayed by black lines with arrow heads. Circles with central black spots show locations of observed Quaternary deformations. Contour lines represent basement elevation in km with respect to sea level. Small asterisks correspond to historical earthquakes having I_0 between VII and VII–VIII while larger asterisks indicate historical earthquakes with $I_0 \geq$ VIII. The dotted rectangle shows the 3-D model surface area.

a consequence, active deformation in western continental Europe is very low. However, internal forces such as residual Alpine slab pull and gravitational forces related to crustal heterogeneities are also proposed to explain part of (Sévrier *et al.* 2004) or the whole (Le Pichon 2004) weak to moderate seismic activity of southeastern France. Despite the description of many metre scale Quaternary faults (e.g. Baize *et al.* 2002), it is generally difficult to link moderate earthquakes with identified faults (Brittany, western Alps and Pyrenees). In regions of slightly higher seismotectonic activity such as Provence, it is sometimes possible to correlate low slip-rate active faults with instrumental, historical, and palaeoseismic activity (Cushing *et al.* 1997; Sévrier *et al.* 1997; Baroux 2000; Guignard *et al.* 2005). This is the case for the NNE-striking Middle Durance Fault System (MDF) which can be traced over 80 km from Aix-en-Provence to the Digne Thrust (Fig. 1). This MDF is made of two fault zones: (1) the Middle Durance Fault Zone (MDFZ) to the North and (2) the Aix Fault Zone (AFZ) to the South (Fig. 1) linked together by a right bend.

In this paper, we perform a critical review of available data on MDF. It includes re-interpretation of seismic sections and investigation of recent microseismic events recorded by a devoted seismic network installed along MDF in 1996. Results deduced from the whole study confirm that a multidisciplinary approach is useful to better assess seismic hazard of active faulting in regions of low to moderate seismicity.

2 GEOLOGICAL AND SEISMOTECTONIC REGIONAL BACKGROUND

2.1 Structural framework

Western Provence mainly corresponds to a Mesozoic shelf basin bounded by deeper basinal conditions to the NE. The regional structural framework can be divided into four major domains (Fig. 1):

(1) *The 'Provence panel'* (Chardon & Bellier 2003 and references herein) corresponds to the West Provence thrust sheet and is characterized by a 5–10-km-thick mostly calcareous Mesozoic and Cenozoic series. It is located between the Nîmes Fault to the West and MDF to the East. To the South, the 'Provence panel' is bounded by several south-verging thrusts such as the Trevaresse-La Fare-Alpilles faults.

(2) *The Baronnies*, north of the 'Provence panel', are made of a Mesozoic marly series accumulated in a deep trough. The Baronnies are limited to the South by the Ventoux-Lure Thrust (VLFZ).

(3) *The Valensole Plateau*, is a Mio-Pliocene foreland basin of Southern Alps characterized by a thin and slightly deformed Mesozoic sedimentary cover. It extends between the MDFZ and the Digne thrust.

(4) The Digne thrust represents the Alpine thrust front where thick marly Meso-Cenozoic series are overthrust on the Valensole basin during Neogene and Quaternary.

2.2 Tectonic evolution

E- and NE-striking major faults are inherited from Late Palaeozoic strike-slip faults (Arthaud & Matte 1974). They were reactivated as normal faults during a Liassic extension controlled by three main faults (Fig. 1): Cevennes, Nîmes and Durance faults (Debrand-Passard *et al.* 1984; Roure *et al.* 1992). These became strike-slip faults during the Pyrenean, Palaeogene, tectonic phase which results, from a N-trending compression. This compression also produced E-striking north-verging folds and thrusts (Clauzon 1984; Villeger 1984). The latter appear mostly ramping off detachment levels that are mainly located within Triassic evaporites and sometimes within Liassic to Oxfordian black shales and Neocomian marls (Benedicto-Esteban 1996; Champion *et al.* 2000; Lacassin *et al.* 2001). Some of these detachments are thought to be anchored in the pre-Triassic basement (Villeger & Andrieux 1987; Roure & Colleta 1996; Chardon & Bellier 2003; Sébrier *et al.* 2004).

Oligocene to Lower Miocene oceanic opening of the Western Mediterranean basin produced fault-controlled continental basins, for example, Manosque-Forcalquier or Vistrenque basins (Benedicto-Esteban 1996). This process increased the strong variation in the sedimentary cover thickness across major regional faults as the MDFZ (Fig. 1). Since Middle Miocene, Alpine convergence has been reactivating all the previously mentioned structures causing inversion of the MDFZ over the Valensole basin. South verging E-trending faults have been reactivated or created during the same period. The Alpine convergence has also been responsible for the reactivation of the Digne thrust and the flexural formation of the Valensole foreland basin (Clauzon 1975; Combes 1984; Leturmy *et al.* 1999; Hippolyte & Dumont 2000). The amount of Miocene to Present crustal shortening is estimated to be on the order of 10 km in the Digne region (Lickorish *et al.* 2002).

2.3 Recent and present tectonic activity

Presently, the Provence region is mainly characterized by a compressional tectonic regime. Evidence of this compression is provided by focal mechanism solutions (Nicolas *et al.* 1990; Baroux *et al.* 2001; Volant *et al.* 2003) and by geodetic analyses (Ferhat *et al.* 1998; Calais *et al.* 2002, 2003; Nocquet 2002; Nocquet & Calais 2004). Reported Quaternary transcurrent, reverse, or thrust faults (e.g. Villeger 1984; Terrier 1991; Ghafiri 1995; Cushing *et al.* 1997; Sébrier *et al.* 1997; Baroux 2000; Dutour *et al.* 2002; Chardon & Bellier 2003; Chardon *et al.* 2005; Guignard *et al.* 2005) also agree with such a compressional tectonic regime characterized by a NNW-to N-trending compression (see review of most of these data in Baize *et al.* 2003). Estimates of slip rates on individual faults range from 0.01 to 0.1 mm yr⁻¹. These slip rates are based on either balanced cross-section (Champion *et al.* 2000), or offsets of geological markers (Chardon & Bellier 2003; Siame *et al.* 2004; Chardon *et al.* 2005) or geodetic studies (Nocquet 2002; Nocquet & Calais 2004).

3 KNOWLEDGE OF THE MDF

3.1 Overall MDF geometry

The MDF separates two different structural domains (Fig. 1): a thick Mesozoic to Oligocene sedimentary cover to the West, and a thin

Mesozoic pile covered by a thick Neogene to Quaternary molasse series to the East. As mentioned above, the MDF is made of two main zones: AFZ and MDFZ (Fig. 1). In cross-sections (Figs 2 and 3) MDFZ is composed of two structures: (a) to the East a high angle west dipping basement fault and (b) to the West structure is a listric normal fault soling within Triassic beds (Roure *et al.* 1992; Benedicto-Esteban 1996; Benedicto *et al.* 1996; Roure & Colletta 1996; Figs 2 and 3).

Several, small-scale, oblique folds are bent northward along the MDFZ. They provide evidence for a left-lateral strike-slip component of a post-Miocene fault movement. This movement caused inversion and bending of the E-striking pre-existing Manosque-Forcalquier basin. Regional-scale E-trending folds (e.g. Lubéron, Trévaresse) are also bent northward along the MDFZ.

In addition, this inversion has produced a west-up, reverse displacement of Manosque anticline. However, the MDFZ central part still shows about 4 km of normal displacement of the basement top, down dropping to the West (Fig. 1). Liassic Tethysian opening and Oligocene to Lower Miocene rifting periods were both responsible for this cumulated normal downthrow (Beaudrimont & Dubois 1977; Roure *et al.* 1992). Subsequently, Neogene to Present deformation has produced the apparent reverse displacement that is exhibited by a vertical upthrow of about 1.5 km postdating Miocene beds (Combes 1984; Terrier 1991; Roure *et al.* 1992).

3.2 Palaeoseismicity

Until the end of the 1980s, the MDF was considered to be an active fault because of its historical and instrumental seismicity. Subsequently, some Quaternary deformation has been reported: striated Würmian conglomerates (Villeger 1984) and a faulted Rissian formation (Terrier 1991) at La Brillanne site (Fig. 1). In addition, a knee fold affecting Quaternary to Holocene torrential debris flow has been observed in the vicinity of Manosque town, near the Valveranne creek (Ghafiri *et al.* 1993; Ghafiri 1995; Sébrier *et al.* 1997). These studies have proposed that the observed deformation occurred roughly between 27 000 and 9000 years ago, during a palaeoearthquake with a coseismic reverse dislocation of approximately 1 m. This knee fold was supposed to be linked to a fault dipping eastward under the Durance Valley. Moment magnitude was estimated between 6.5 and 6.9 (Sébrier *et al.* 1997). Investigations dealing with geophysical imaging and cosmogenic dating near Manosque suggested a possible vertical offset of the Upper Pleistocene Durance terrace (Siame *et al.* 2004).

3.3 Historical seismicity

Historical seismicity is documented with the SISFRANCE French historical database (see Levret *et al.* 1994; Lambert *et al.* 1996; Scotti *et al.* 2004). Regarding the MDF area, a pseudo-recurrent seismic activity has been reported since the 16th century, with earthquakes producing epicentral intensities ranging from VII to VIII MSK. The strongest events were located near the city of Manosque (13/12/1509 – Io = VIII and 14/08/1708 – Io = VIII). Weaker earthquakes occurred near Beaumont de Pertuis (20/03/1812 – Io = VII–VIII) and near Volx (14/05/1913 – Io = VII–VIII). Much weaker events associated with intensities ranging from V to VII were also reported: 1835 – Io = VI; 1852 – Io = V–VI; 1858 – Io = VI–VII; 1897 – Io = VI; 1938 – Io = V. These events were probably shallow given the limited geographical distribution of reported intensities. Some recent studies of the 1708 earthquake sequence further support a hypocenter depth shallower than 5 km

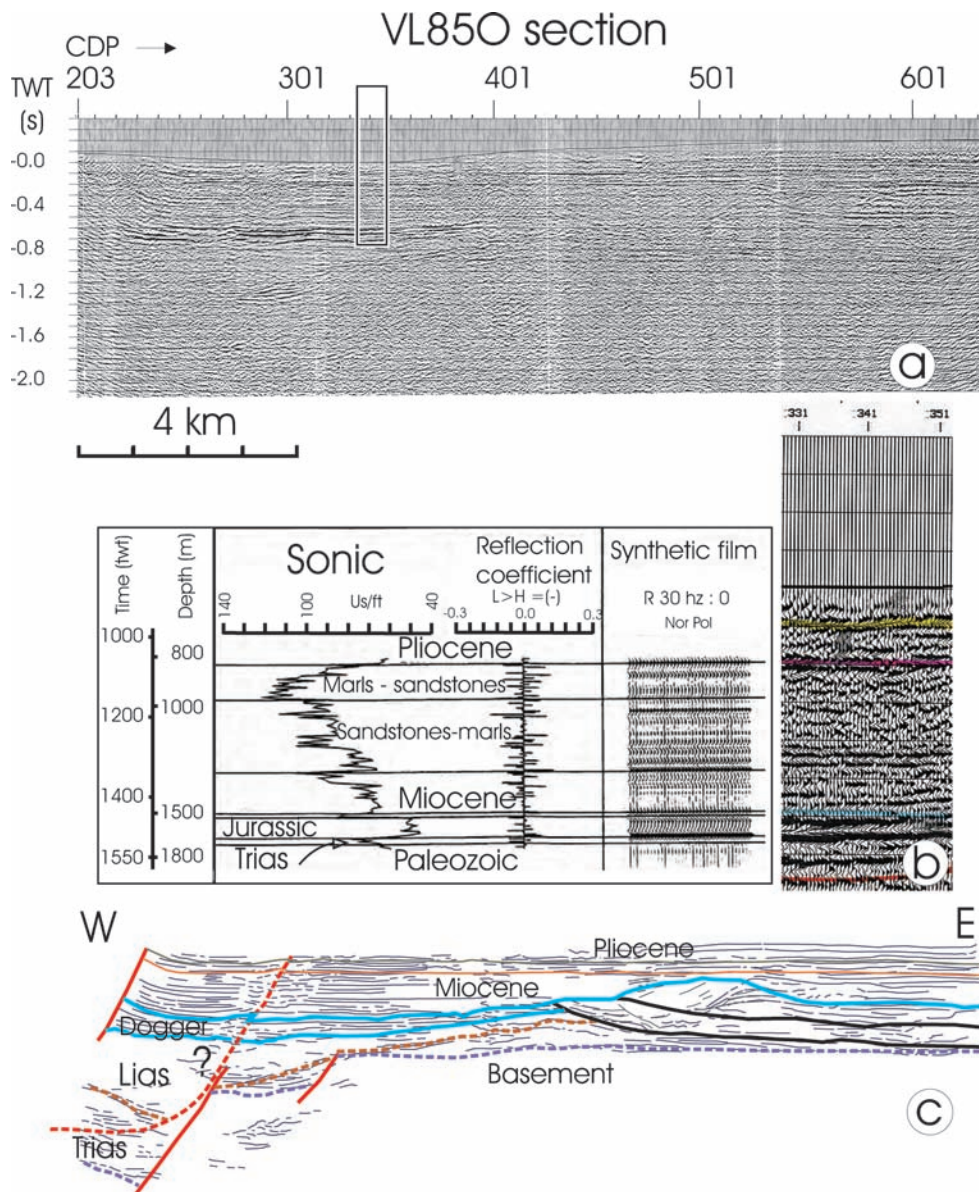


Figure 2. Example of the procedure applied to data used to construct the structural model: (a) Migrated seismic section VL850, (b) Synthetic film used to identify reflectors and correlation with part of section VL850 (rectangle on Fig. 2a) and (c) Line drawing.

(Quenet *et al.* 2004; Baumont & Scotti, personal communication, 2006). Finally another earthquake occurred further North in the region of La Motte Du Caire (19/05/1866 – $I_0 = \text{VII-VIII}$). This event took place near the NNE-trending Vermeihl crustal fault (Fig. 1), which is characterized by faulted basement outcrops. Rousset (1978) suggested this fault belonged to the northern extension of MDF.

3.4 Instrumental seismicity

Both national networks LDG/CEA and RENASS have recorded a moderate seismic activity along MDF since 1962. Approximately 50 earthquakes are listed in the LDG/CEA/LDG catalogue with M_L ranging from 1.5 to 3.0 and only one event with M_L slightly greater than 3.0. The RENASS catalogue lists of 65 events for the 1980–2004 period with M_L ranging from 1.5 to 3.4 (RENASS: <http://renass.u-strasbg.fr/>). All of these earthquakes were located in a 10 km wide strip along MDF. In 1993, in order to study the seismic behaviour of an active fault in a moderate seismic activity context,

the IRSN (French Institute for Radioprotection and Nuclear Safety) began installation of a seismic network ('the Durance network') surrounding the MDF area. Since 1996, this network has been devoted to monitoring the MDF and has consisted of 12 velocimeters and 18 accelerometers spread over a $30 \times 60 \text{ km}^2$ area centred on the fault system (Volant *et al.* 2000). The velocimeters are designed to record low magnitude events (down to $M_w \sim 1$) to investigate the microseismicity of the fault. So far, the Durance network has recorded a weak seismic activity—for the 1999–2006 period, about 70 seismic events with moment magnitudes (M_w) ranging from 1.0 to 2.2 have been located in the same 10 km wide strip along the MDF. The epicentres are relatively well located except in the North where a few events occurred under the Valensole Plateau.

3.5 Geodetic data

The National Geodetic Network (RENAG, <http://renag.unice.fr/regal/>) has two permanent GPS stations located on either side of

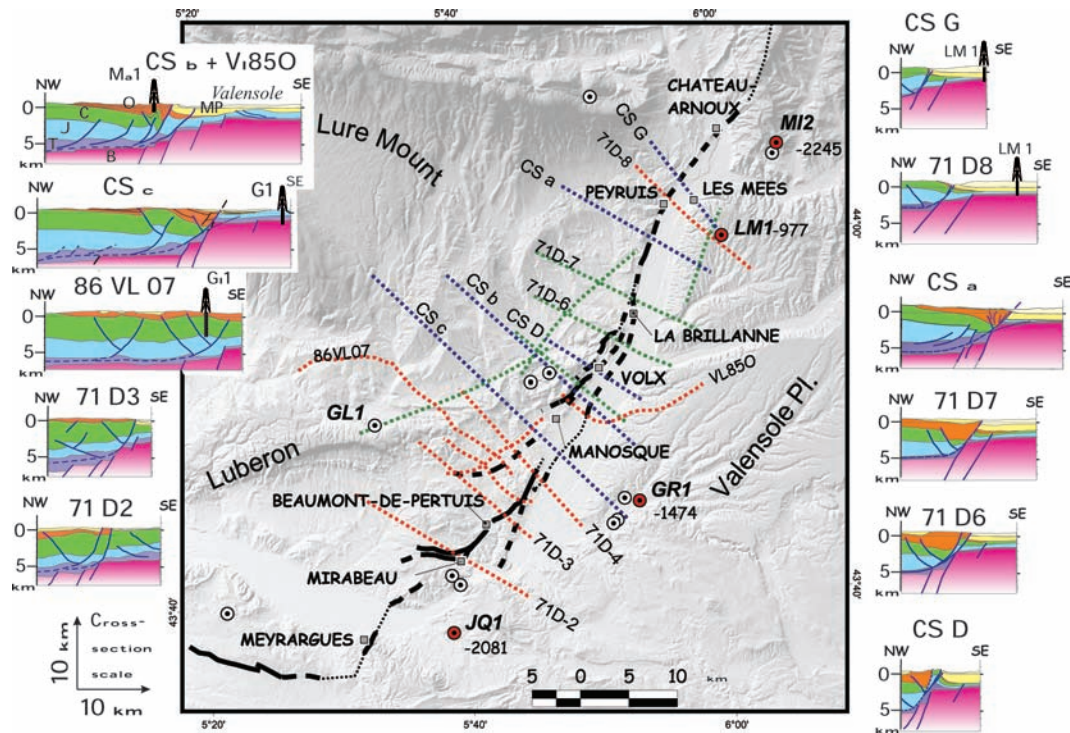


Figure 3. Location map of seismic surveys, geological cross sections, boreholes, cities and surface fault trace of MDF (full, dashed and dotted lines indicate low, medium and high uncertainties in fault trace location, respectively). Boreholes are indicated by circles with central black spots. Red circles correspond to boreholes that reached basement top and negative numbers beside are their depth with respect to seal level. (Borehole names: MI2 = Mirabeau 2; LM1 = Les Mées 1; GL1 = Grand Luberon 1; GR1 = Gréoux 1; JQ1 = Jouques 1). The interpreted cross sections obtained along the MDFZ from seismic section interpretations and complementary geological sections are displayed on each side of the location map (layer labelling on top left corner cross section: B for basement, T for Trias, J for Jurassic, C for Cretaceous, O for Oligocene and MP for Mio-Pliocene series).

MDF. They are located 5 km east and 10 km west of the MDFZ trace. Data have been continuously recorded since 1998. The far field velocities inferred from base-line shortening (Azimuth N169°E; distance 28 km) between these two stations are lower than 1 mm yr⁻¹, with the results yielding a shortening of 0.1 mm yr⁻¹ ± 0.6 mm with a 95 per cent confidence level (Baize & Nocquet 2006).

4 SEGMENTATION AND 3-D GEOMETRY OF MDF

In a region of low seismic activity, seismic hazard assessment related to a fault system is generally approached with only a fault segmentation description combined where possible with a palaeoseismic study. For the MDF area, seismic exploration data are also available and cross sections of the fault system can be obtained from seismic line interpretations and geological data. These cross sections help to better illustrate the fault segmentation and 3-D geometry of the MDF and consequently help to constrain the fault seismogenic potential.

4.1 Presentation of the available seismic sections surveying MDF

In the MDF region, two main seismic campaigns were carried out by oil companies: ELF in 1971 and TOTAL in 1985–1986. We obtained from the COPAREX Company, four hard copies of migrated seismic sections belonging to Total. In addition, three seismic sections from the ELF 1971 campaign reprocessed and migrated by CGG Company were made available by the CEA/Cadarache Centre. A

total of seven seismic sections were interpreted and all include time migration and CDP numbers on the horizontal axis.

Seismic analyses and interpretations were either presented in internal reports (Cabrol 1985; Biondi *et al.* 1992) or partly reported by Benedicto-Esteban (1996). Roure *et al.* (1992) and Roure & Colletta (1996) used the same data to describe the structural mechanism of fault inversion in the Alpine and Pyrenean forelands.

Data acquired in the 1980s were of good quality and valuable features about structural organization were obtained from the corresponding seismic sections. In contrast, data acquired in the 1970s were of poorer quality. Other seismic sections coming from the above-referred unpublished reports were also used. These additional sections are of poor quality they provide, however, a few valuable indicators for locating the MDFZ and interpreting its geometry.

4.2 Correspondence between seismic reflectors and geological layers

The interpretation process started by identifying characteristic seismic reflectors using information deduced from boreholes. From different types of logs (sonic, density, resistivity, seismocoring or CVL) propagation velocities values were obtained. They were used to produce synthetic seismograms generated by convolving the reflectivity derived from digitized logs with a wavelet. The comparison between those seismograms and seismic sections allowed the determination of seismic reflectors (Fig. 2).

The last step of the interpretation process consisted in converting the original time seismic sections into depth sections. In order to make this conversion, propagation velocities (*V_p*) of the various

geological formations are required. Most of these velocities were deduced from the previously cited logs. For the others, values were obtained by estimating formation thicknesses from geological data and associated two-way traveltimes from migrated seismic sections. Since horizontal axes of sections contain CDP numbers, the time interval measured between two interfaces of a given formation corresponds to the two-way traveltime. The ratio of its thickness over the one-way traveltime is our V_p estimate.

Unfortunately, the different migration techniques applied by the TOTAL and CGG companies lead to significant differences in depth between similar reflectors. Therefore some 'interpreted' geological cross-sections deduced from geological maps and published cross-sections (e.g. Benedicto-Esteban 1996) had to be integrated to reconcile those discrepancies. Overall nine geological interfaces could be pointed out on the Elf sections and 7 on those of Total. In both sets, basement or an interface located near the top of the basement was identified (Fig. 3).

4.3 Fault trace mapping and segmentation

Until the late 1990s, knowledge of the MDF fault trace was limited. At that time, existing geological maps (1/50 000 scale) displayed very few local fault strands and the 1 000 000 scale French geological map showed MDF as a dashed line. Some authors proposed a preliminary mapping of MDF but with great uncertainties (Combes 1984; Terrier 1991).

Taking advantage of results from studies completed since the 1990s (e.g. Cushing *et al.* 1997; Baroux 2000; Guignard 2002; Lebatard; 2003; Siame *et al.* 2004; Guignard *et al.* 2005; Nguyen 2005), field investigations and the above listed seismic section interpretations, we performed a synthesis that resulted in an updated mapping of MDF (Fig. 3).

Locations of near surface faults were obtained from a variety of data: (1) geological maps, (2) aerial and satellite images, (3) DEM analysis of slopes anomalies, (4) near surface geophysical surveys, (5) location of geomorphic anomalies (e.g. stream deviations) and (6) Quaternary deformation features.

Special attention was paid to locate the surface fault trace from upward projections of the faults observed at depth on seismic sections. This mapping has allowed us to propose the seismotectonic segmentation presented in Fig. 4 and detailed in Appendix A. Boundaries between segments are mainly defined by changes in mean fault-strike.

4.4 3-D geometry of MDF

4.4.1 Previous research on 3-D geometry

As previously suggested from cross-section views by Roure *et al.* (1992), Roure et Colletta (1996) and Benedicto-Esteban (1996), the crustal part of the MDFZ is characterized by a staircase shaped faulting affecting the basement top. The western part of the MDFZ is a listric decollement curving horizontally within Triassic evaporite beds.

A seismotectonic hypothesis considers the MDF as an active left-lateral ramp separating an autochthonous domain to the East from the detached sedimentary series to the West (Benedicto-Esteban 1996; Champion *et al.* 2000). Active deformation is thus restricted to the sedimentary cover and basement faults remain inactive. An alternative hypothesis suggests the involvement of basement faults in regional deformation (Chardon & Bellier 2003; Sébrier *et al.* 2004).

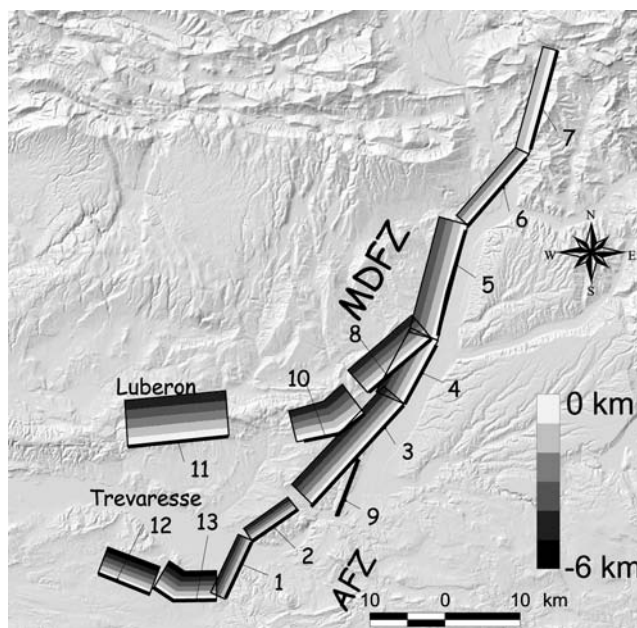


Figure 4. Map of simplified MDF segmentation. All segments are numbered, details for each of them are given in Appendix A. Fault plane depth is indicated by a grey scale (from 0 to 6 km depth).

4.4.2 Insights from our analysis of seismic sections

The construction of several cross sections (Fig. 3) confirms the structural organization proposed by Benedicto-Esteban (1996). However, the geometry imaged by these cross sections is not sufficient to fully assess the fault seismogenic potential because this geometry cannot provide evidence to distinguish whether fault activity involves both the basement and listric faults or is restricted to the listric faults only. This ambiguity is illustrated on line VL850 (Fig. 2) where interpretations do not allow the choice between these two hypotheses. Another way of investigating fault activity is to determine locations of seismic events with respect to the previously described crustal fault organization. Therefore, the seismicity recorded by the Durance network was used to address the question about basement fault activity.

5 MICROSEISMIC ANALYSIS

5.1 Construction of a 3-D velocity model

Prior to this study, seismic events around the MDF were located with a 1-D velocity model. However, this 1-D velocity model is not representative of the 3-D complexity of geological structures in the MDF region. Thus a 3-D velocity model was needed in order to obtain reliable hypocenter locations and consequently improve the knowledge about fault activity in the basement. The first step in developing a 3-D velocity model was to build a 3-D structural model describing the main geological interfaces. These interfaces were obtained by two methods: (1) interpolation between scattered data points and (2) draping over interfaces defined on seismic sections. The first method was applied far from seismic lines using geological maps and interpreted geological sections. Closer to MDF, a draping technique was used between all available seismic sections in order to better image the topography and dip of the faults.

In a second step once the geometry of the main interfaces was established, the P -wave velocities determined in Section 4.2 were attributed to each layer of the structural model (Fig. 5). This geometry

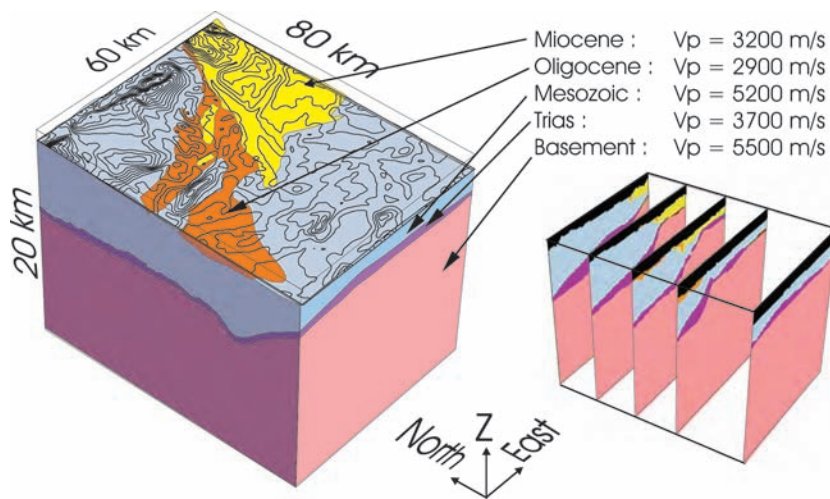


Figure 5: 3-D velocity model with its P -wave velocities V_p (Left 3-D numerical bloc where topography is represented by contour lines, right: cross-section views).

was input into the GOCAD™ modelling software. The last step consisted in outputting with GOCAD the velocity distribution to a 3-D grid using unitary cubes. Each cube has edges of 200 m and is assigned constant P -wave slowness ($1/V_p$) corresponding to 3-D location (x, y, z) of the cube centre. The velocity model consists of about 13 million elementary cubes. The resulting 3-D model remains a simplified velocity model, with some large uncertainties and includes expert judgment. Nevertheless, we consider it to be much more appropriate for the complex structure of the MDF than the previously used 1-D model.

5.2 Event selection

Relocation of 155 events recorded by the Durance network between 1999 and 2006 were obtained using the 3-D Velocity model presented above and the Non-Linear Location (NonLinLoc) program (Lomax *et al.* 2000; Lomax & Curtis 2001; Lomax 2005) (Fig. 6). This software is capable of computing traveltimes and probabilistic, non-linear, global-search earthquake locations in the 3-D velocity model. The combination of the 3-D velocity model and the NonLinLoc software minimizes biases and uncertainties in the epicentre and focal depth estimations and produces comprehensive solution error information, such as maximum likelihood hypocenters, probability density function for the hypocenter location and error-ellipsoids (68 per cent confidence ellipsoid). All of this solution information is critical to make robust inferences about location and depth of buried active faults. Moment magnitudes (M_w) for the relocated events were computed from long-period plateaus of displacement spectra (Nechtschein 2003; Volant *et al.* 2003). The magnitudes ranged from $M_w = 1.0$ to 3.0, indicating weak seismic activity in MDF region during a 7-yr study period. Some of the lowest magnitude events were only detected by two or three stations, consequently their locations are poorly constrained, leading to uncertainties in depth of several kilometres. For a refined structural analysis, absolute and relative location uncertainties were discarded. To minimize event location errors, we developed station corrections using an iterative procedure to accumulate mean station residuals. We then performed a selection to retain the best located events using the following criteria: (i) at least 5 arrival times used for location, (ii) maximum confidence-ellipsoid, semi-axis length ≤ 2 km, and (iii) maximum azimuthal gap

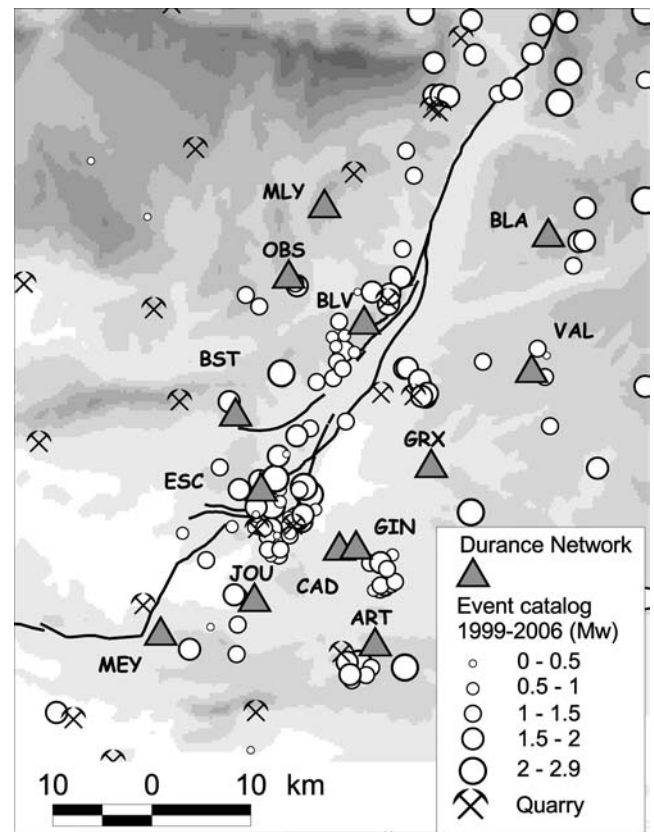


Figure 6. Location map of 155 events recorded by the Durance network for the 1999–2006 period; quarry blasts are included.

$\leq 270^\circ$. From the 155 events located, 90 were selected with those criteria.

A final selection step was the removal of quarry blasts from these 90 events using signal identification and available information from quarry managers. The final event set consisted of 59 earthquakes (Fig. 7 and Appendix B). The location errors are quantified by the maximum confidence-ellipsoid, semi-axis length (Se_1, Se_2, Se_3 in Appendix B); for most events the maximum semi-axis length (Se_3) is oriented nearly vertically. Thus, in Appendix B, the uncertainty

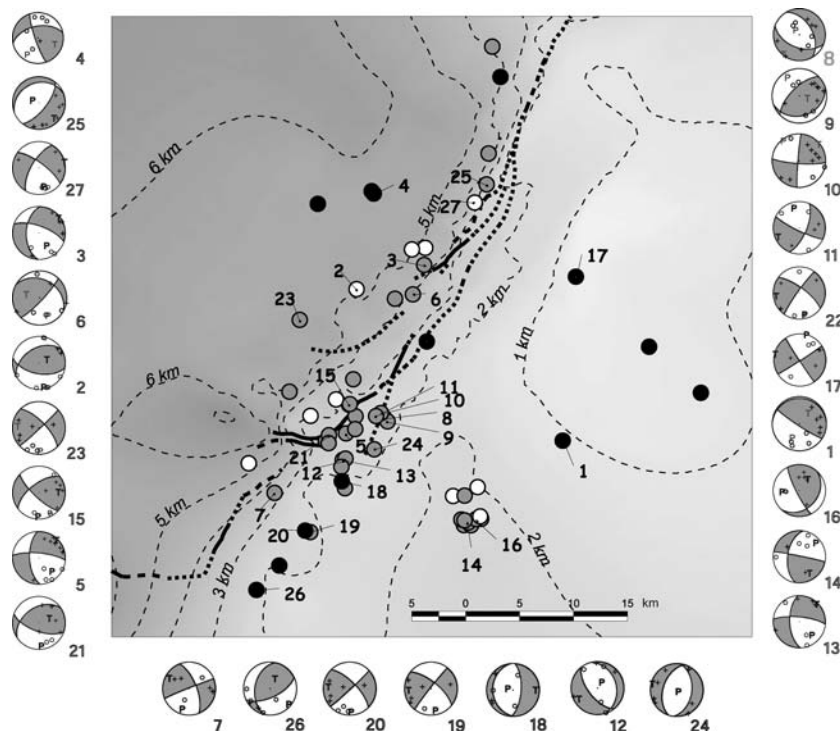


Figure 7. Location map of the 59 best located events around MDF. Circle colours indicate different event depths with respect to basement top (black: events located at least 2 km below basement top; grey: events located less than 2 km above or below basement top; white: events located more than 2 km above basement top). Dashed contours indicate depth of basement top). Focal solutions could be computed for numbered events only, corresponding focal mechanisms are represented around the map.

in depth is very close to \pm Se3 km. The mean of the Se3 values in Appendix B is 1.0 km. Focal mechanisms were computed for 27 events having sufficient first motion readings using the FPFIT software (Reasenber & Oppenheimer 1985). Due to the small number of stations used to determine some focal mechanisms, multiple solutions were obtained for about half of these 27 events (Fig. 7 and Appendix C).

5.3 Seismicity location and active fault size

The distribution of the selected epicentres (Fig. 7) shows that the seismicity around the MDF is less diffuse than suggested by national networks (e.g. Baroux *et al.* 2001). West of MDF, under the Provence panel, the level of seismic activity is very low. Similarly, only a few events occurred under the Valensole Plateau, 10–15 km East of the MDFZ. The majority of events occurred in the vicinity of MDF along a 50×10 km² strip between Peyruis and Meyrargues (Figs 6 and 7) with a higher density of earthquakes between segments 3 and 7. The southernmost events in this strip are located up to about 10 km southeast of the mapped faults. Most of the events located in the vicinity of MDF are close to the surface with depths shallower than 4 km (all depths in this paper are indicated with respect to sea level; Fig. 8), which indicates that the present-day seismicity associated with MDF is mainly situated within the sedimentary cover.

There is also a cluster of events located around Mont-Major, a few kilometres southeast of CAD and GIN seismic stations (Figs 6 and 7). Events in this cluster have shallow depths, between 1 and 2 km and may be interpreted as southwest verging Mont-Major thrust activity. No Quaternary deformation evidence has previously been reported for this location.

Some deeper seismicity is also found. Three events deeper than 8 km occurred under the northern limb of the Luberon-Manosque

anticline. In the prolongation of segment 9 (near Jouques), five events are aligned with depths ranging from 4 to 9 km. In this area, a relatively deep earthquake (M_L $1d_g = 2.9$, $h = 9$ km) occurred in 1997 (Volant *et al.* 2000). Since the Jouques borehole located in the area reached the basement at a depth of 2065 m, these events probably occurred within the basement. Such a zone of deep seismicity could reveal the existence of an active crustal fault (e.g. NNE-trending Jouques Fault).

The deepest events occurred under the Valensole Plateau with depths ranging from 8 to 15 km. They are associated with crustal deformation which might be related to the frontal activity of SW-verging crustal thrust (Leturmy *et al.* 1999; Hippolyte & Dumont 2000) located 15 km to the north. This structure has previously been identified from oil exploration surveys (Dubois & Curnelle 1978) which induces the Lambrussier and Mirabeau anticlines in the northern Valensole Plateau (Fig. 1). Moreover, two deep earthquakes (8 and 10 km deep) with reverse mechanisms occurred in this area in 1984 (Nicolas *et al.* 1990; Baroux *et al.* 2001), these events suggest active thrusting under the northern Valensole Plateau.

5.4 Earthquake fault-plane solutions and fault kinematics

The 27 focal mechanisms obtained with FPFIT are shown in Fig. 7. For events having multiple solutions, a single mechanism has been selected based on either the nodal-plane best-fit determined using inversion of seismic slip-vector (see next section) or on the computed solution quality based on the highest station distribution ratio (STDR: see Reasenber & Oppenheimer 1985). Nevertheless some of the solutions (Fig. 7 and Appendix C) remain poorly constrained, that is, STDR < 0.5 (events 9, 18, 21 and 26).

The majority of the 27 mechanisms are consistent with strike-slip faulting in agreement with left lateral displacement along the MDF.

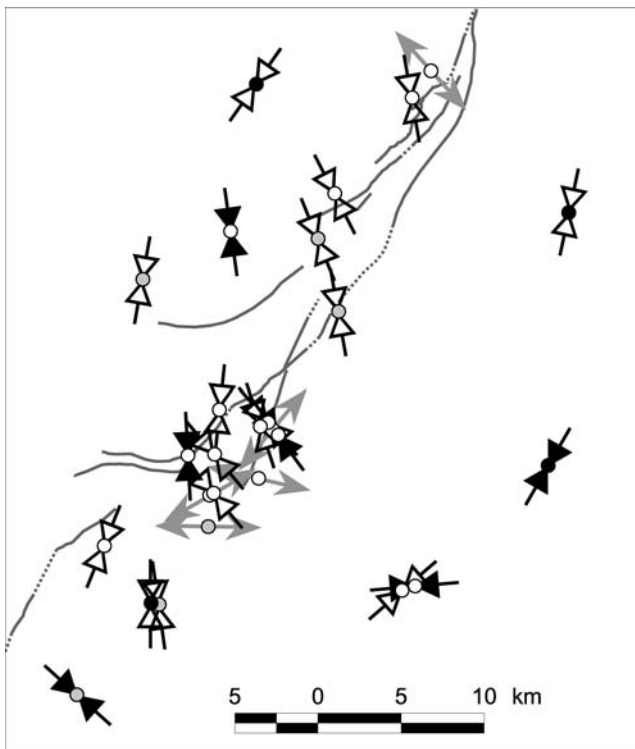


Figure 8: *P*- and *T*-axes distribution, deduced from focal solutions (see Fig. 7 for event numbers). Arrow colours indicate different types of faulting mechanisms (black: *P*-axes corresponding to reverse faulting mechanisms; white: *P*-axes corresponding to strike slip mechanisms; grey: *T*-axes of normal faulting mechanisms). Dot colours correspond to absolute depth with respect to sea level (black: below 6 km; grey: between 3 and 6 km and white: shallower than 3 km).

A few events with reverse focal mechanisms are spread out over the whole study area, and several events with normal mechanisms are concentrated near segments 2 and 3. The presence of these normal events may be interpreted as a local reorientation of the main stress direction near the termination of segment 3.

The difference in *P*-axes orientation (N to NNE-striking) (Fig. 8) between the basement and the sedimentary cover could indicate stress decoupling between thin-skinned tectonics (thrust sheet motion of the ‘Provencal panel’) and deep-seated deformation. Such stress decoupling has been described in the same context for the Northern Jura thrust belt (Becker *et al.* 1987). The distribution of *P*-axes near the Luberon fold suggests some possible thrusting activity. An event that occurred south of the Concors fold (event 26) has a reverse solution with a N-130°E-trending *P*-axis, since it has a very low STDR value this solution is discarded.

Finally, two focal mechanisms were computed for the Mont-Major cluster. They are difficult to interpret because their *P* axes are perpendicular to the N-trending *P*-axes of the majority of events. Nevertheless one focal solution shows a low-angle, nodal plane which could be related to either the thin-skinned tectonics or local halokinetic behaviour. In this area, large evaporitic Triassic windows crop-out.

5.5 Inversion of seismic slip-vector data set to determine the current stress state

Several algorithms (e.g. Vasseur *et al.* 1983; Gephart & Forsyth 1984) are available to compute stress states. From a robust data set, these algorithms yield similar results (e.g. Mercier *et al.* 1991).

To compute the stress states responsible for the present seismic activity in the studied area, quantitative inversions of earthquake focal mechanisms were performed using the method proposed by Carey-Gailhardis & Mercier (1987, 1992). This method and its stress axis uncertainties are described in detail by Bellier *et al.* (1997) and Baroux *et al.* (2001). For this inversion technique, the slip (*s*) for a given focal solution is represented by a vector corresponding to the rake of each nodal plane. The slip is assumed to occur in the direction of the resolved shear stress (τ) on each fault plane, the fault plane being a pre-existing fracture. The inversion computes a mean best-fitting deviatoric stress tensor from a set of fault slip vectors by minimizing the angular deviation between a predicted slip vector (maximum shear τ) and the observed slip vector (*s*) deduced from the corresponding focal mechanism (Carey & Brunier 1974; Carey 1979).

The application of the above described method requires the correct nodal plane to be selected from the 2 slip vectors obtained with a focal mechanism. The magnitudes of the earthquakes recorded by the Durance network mainly range from 1.2 to 2.2. Consequently, it is difficult to select the nodal planes from structural criteria because these low magnitude earthquakes correspond to dislocations propagating along a few tens of metres only. These small ruptures can occur on major faults as well as minor ones. The methodology consists in selecting the slip vector with a numerical approach based on the computation of the *R* ratio defined as $R = (\sigma_2 - \sigma_1) / (\sigma_3 - \sigma_1)$. In Bott’s model (1959), only one of the two possible slip vectors of a focal mechanism solution agrees with the principal stress axes having an *R* ratio between 0 and 1 (see appendix A in Baroux *et al.* 2001). In our study, this numerical approach was applied to select the appropriate plane for 25 events (Appendix C), those of Mont Major being discarded. Some events had multiple focal solutions. Overall 94 nodal planes were considered.

The inversion was performed in two steps. The first one consisted in inverting the whole data set in order to approach an optimized stress tensor. For the second step, only nodal planes having both criteria ($0 < R < 1$ and $\tau, s < 30^\circ$) were inverted. Those nodal planes corresponded to 19 events located either in the cover sheet of the MDF (events 2, 3, 5, 6, 7, 9, 10, 11, 13, 15, 19, 21, 23 and 27) or within the basement (events 1, 4, 17, 20 and 22).

The resulting deviatoric tensor shows a strike-slip regime characterized by a N165°E-trending σ_1 , a N74°E-trending σ_3 and an *R*-value of 0.58 (Fig. 9a). This stress state is consistent with the composite focal mechanism obtained with the FPFIT code (Fig. 9b) and agrees with that of Baroux *et al.* (2001). The latter was computed with five nodal planes selected from larger magnitude events ($2.9 \leq M \leq 4.1$). It indicated a strike-slip stress state with a N158°E-trending σ_1 and an *R* value of 0.49.

Most of the seismic events excluded after the first step of the inversion would indicate a NNE-trending extension. This data set was not inverted for the stress tensor because of the small number of remaining events. These mainly lie in an area located around the southern termination of segment 3 (Fig. 4—south of the bend), suggesting a *P*-axis rotation in relation with a local stress-state change (Fig. 8).

6 SEISMIC HAZARD ESTIMATION FOR MDF

6.1 Maximum moment magnitude

Our results for the MDF suggest that this fault system can be regarded as a set of sources capable of producing significant

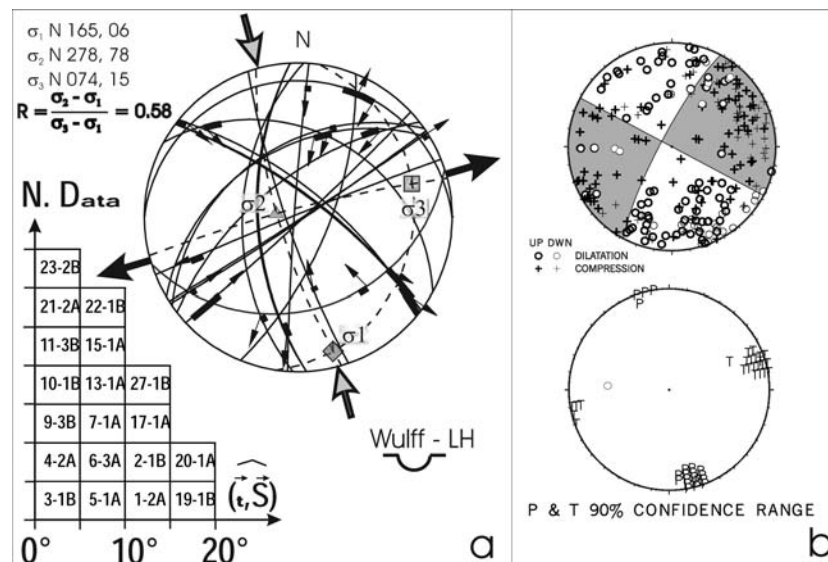


Figure 9. (a) Stress state and deviatoric tensor obtained from focal mechanism inversion. Arrows attached to fault planes show the slip-vector directions (Wulff stereonet, lower hemisphere). Grey and black arrows indicate σ_1 and σ_3 axis directions, respectively. The histogram gives the angular deviation between the predicted slip vector ' τ ' and the observed slip vector ' s ' for a given nodal plane. Nodal planes are listed in Appendix C. For example, plane 6-3A corresponding to focal mechanism number 6, solution 3 and nodal plane A, has an angular difference (τ, s) between 5 and 10° . (b) Composite solution deduced from P wave first motion of the 27 events having focal solutions (top) and corresponding P - and T -axes distribution (bottom).

earthquakes. Although the Valveranne palaeoseismic evidence mentioned in Section 3.2. (Ghafiri *et al.* 1993; Ghafiri 1995; Sébrier *et al.* 1997) is isolated and not located exactly on one of the major faults it nevertheless suggests potential for large earthquakes.

Estimates of maximum magnitude and fault behaviour may be derived through numerical simulations or direct application of empirical relationships. The latter links segment size and/or source area with maximum earthquake magnitude (e.g. Wells & Coppersmiths 1994; Hanks & Kanamori 1979). The deterministic assessment of the source geometry makes the evaluation of the earthquake size possible using different scenarios. The fault segmentation and geometry described above have already been used in a simplified version to obtain numerical simulations of spontaneous dynamic rupture propagation using a logic tree approach (Aochi *et al.* 2006). The results of these simulations show magnitudes ranging from 6.3 to 6.9 if it is assumed that the deepest parts of main segments reach the basement. The most probable events have a probability of occurrence greater than 20 per cent and correspond to events either along a single segment ($M_w = 6.3$) or along three segments ($M_w = 6.8$). This simulation used a physical approach therefore no return period could be associated with those events.

For the southernmost part of the MDF most of the microseismic events occurred in the sedimentary cover. This is consistent with a decollement within Triassic salt as proposed by Benedicto-Esteban (1996) and Le Pichon (2004). Considering this hypothesis, the source dimensions cannot exceed $18 \times 6 \text{ km}^2$ where 18 km is the maximum segment length and 6 km corresponds to the width of a listric fault reaching Triassic beds (Figs 3 and 4). Application of the Wells & Coppersmith relationship for strike slip faulting with these parameters results in a maximum individual magnitude of 6.0 ± 0.2 for each segment. With the Hanks & Kanamori relationship, this magnitude upper bound is equal to 6.1 considering a 0.5 m dislocation. For this last calculation the shear modulus μ was required. It was estimated to be around $2 \times 10^{11} \text{ dyne cm}^{-2}$ from density and S -wave velocities of the sedimentary cover. If mean instead of maximum segment length is considered, 12 km must be

used instead of 18. In this case, for a 5 km fault plane, the Wells & Coppersmith relationship results in a magnitude of 5.8 ± 0.2 . Hanks & Kanamori relationship also gives 5.8 for the same 0.5 m dislocation. All magnitude values are close to those proposed by Chardon *et al.* (2005) on the Trevaresse active thrust.

6.2 Slip rate and recurrence

Ten years ago, the fault slip rates in southeastern France including those of the MDF were not known. From the Valveranne palaeoseismic evidence (Sébrier *et al.* 1997), the old geological marker displacements, the geophysical markers offsets and the permanent GPS survey, many techniques were applied to estimate short and long term slip rates on the MDF (e.g. Baroux 2000; Bellier *et al.* 2004; Cushing *et al.* 2004). Nowadays, it is widely accepted those slip rates are lower than 0.1 mm yr^{-1} . From cosmogenic dating and geomorphic analyses, Siame *et al.* (2004) obtained a slip rate that ranged from 0.01 to 0.07 mm yr^{-1} for the last million years. This range of values is coherent with integrated GPS monitoring (Baize & Nocquet 2006). The slip velocities are essential to determine whether or not the case of active fault rupturing has to be regarded in seismic hazard assessment.

In order to assess hazard related to fault activity, the characteristic earthquake model (see Schwartz & Coppersmith 1984), is considered. In such a model, maximum magnitude is estimated from the size of a given segment. Then using the relationship of Wesnousky (1986), a return period is calculated. This model is generally applied in highly seismic zones (i.e. Wesnousky 1986) and remains questionable for the case of slow active faults. Nevertheless we use it as a simplified approach even if the behaviour of each fault segment is unknown. This approach has been applied with the hypotheses of Section 6.1. For an earthquake of magnitude $M_w = 5.8$, with an average slip rate of 0.1 mm yr^{-1} , a 12 km long mean segment and a fault plane width of about 5 km, the return period is 4700 yr. On the other hand, for an event of $M_w = 6.1$, with a slip rate of 0.1 mm yr^{-1} , a 18 km long segment and a fault plane width of about 6 km, the

return period is 7340 yr. The involvement of more segments in the rupture process would lead to an increase in magnitude and return period. For instance, a segment rupturing combination involving segments 3, 4, 5, 6 and 7 activates a 340 km² rupture surface area. The return period is then estimated at 9280 yr for a magnitude $M_w = 6.5$ with a 0.9 m dislocation considering a slip rate of 0.1 mm yr⁻¹. This scenario probably corresponds to the upper bound of predicted magnitudes.

7 DISCUSSION AND CONCLUSION

Numerous studies performed during the last decade including re-interpretations of seismic sections, geomorphological analyses, palaeoseismicity studies, near-surface geophysical surveys, cosmogenic nuclides dating, geodetic measurements and seismological investigations, have been jointly analysed to better understand the seismotectonic behaviour of the MDF in order to reassess seismic hazard in the Provence region.

The results obtained from this multidisciplinary approach allowed the construction of a segmentation model of the MDF composed of nine segments with lengths ranging from 8 to 18 km. In addition, a 3-D velocity model mainly obtained from seismic section interpretations has been developed to locate microseismic events recorded by the Durance Network between 1999 and 2006. Most of the hypocenter locations are shallow and therefore in the vicinity of the MDF the microseismic activity mainly lies in the sedimentary cover suggesting that active segments reach Triassic evaporitic beds. These results agree with the geometry proposed by Benedicto-Esteban (1996). However, a few microseismic events recorded by the Durance network have been located deeper than the basement-cover interface. Most of them lie either to the East (Valensole Plateau) or to the West (Luberon Range and Vaucluse Plateau) of the MDF. This deeper seismicity indicates that part of the active deformation is taking place within the pre-Triassic basement.

From the recorded microseismicity, 27 focal mechanisms have been computed. Overall, they show a dominant left-lateral strike-slip faulting behaviour with a roughly N-trending compression that seems to occur in both the sedimentary cover and the basement. Therefore, focal mechanisms indicate that the NNE-striking MDF acts as a southward transfer zone of the external Alpine front in Western Provence between the NNW-striking Digne thrust, and the south verging Trevaresse and Les Costes thrusts. Data analyses also indicate that the link between the Digne thrust and the MDF cuts across the northern Valensole Plateau. This link would correspond to a blind active basement fault zone that is associated with the Lambrussier and Mirabeau anticlines. The presence of this blind fault zone would also suggest that the northern MDF is not currently active and explain why MDF surface trace is difficult to observe. In addition, small variations in *P*-axes orientation (N- to NNE-striking) between the basement and the sedimentary cover could indicate a stress decoupling between thin-skinned tectonics (thrust sheet motion of the 'Provence panel') and deep-seated deformation. Finally, a few mechanisms display thrusts or normal faults, these can be explained by local stress deviations due to fault terminations and/or folding locally perturbed by salt tectonics.

The seismogenic potential of the MDF has been roughly estimated from segmentation and geometry obtained in this study. Resulting source sizes and estimated slip rates imply that the magnitude upper limit ranges from 6.0 to 6.5 with a return period of a few thousand years.

In the context of regions of low strain rates, the present study shows that, when available the combination of 3-D fault geometry

imaging and accurate microseismic location provides a robust approach to analyse active fault sources and consequently produces a more refined seismic hazard assessment.

Considering seismic hazard at the regional scale of Provence, the occurrence of microseismicity below the sedimentary cover indicates that further investigations should be carried out to identify and characterize potentially seismogenic blind thrusts within the basement. Such basement faults have been previously proposed in both Western and Eastern Provence (Dubois & Curnelle 1978; Lickorish & Ford 1998; Hippolyte & Dumont 2000; Laurent *et al.* 2000; Larroque *et al.* 2001; Bigot-Cormier 2004; Sébrier *et al.* 2004). However these faults are too poorly understood to be integrated in the assessment of seismic hazard in Provence. A similar approach to the one conducted on the MDF should be devoted to such blind thrust sources.

ACKNOWLEDGMENTS

This study was supported by IRSN funds and benefits from other studies performed through several cooperative agreements with Orsayterre, CEREGE, Géosciences Azur and the SAFE project (Slow Active Faults in Europe; EVG1-000-2005). This work has also benefited from the French National Program ACI-FNS 'Aléas Changements Globaux' (IRIS-2 project), and from the ISIS program that provided SPOT images ((c) CNES). The authors wish to thank B. De Voogt, T. Rosique, S. B de Berc, S. Baize, E. Baroux, T. Ait Ettajer, P. Combes, O. Scotti and D. Baumont for their contributions and L. Siame, D. Chardon, B. Meyer, F. Hollender, F. Bonilla, X. Le Pichon and P. Thierry for fruitful discussions. The authors would also like to thank M. Canard and Mervoyer from COPAREX who provided the four TOTAL seismic sections used in this study, M. Buisson from LUNDIN-PETROLEUM who authorized the publication of part of the VL850 line and the CEA/Cadarache for providing four ELF seismic sections. Finally the authors are grateful to the editor and two anonymous reviewers for providing comments that greatly improved the manuscript.

REFERENCES

- Aochi, H., Cushing, M., Scotti, O. & Berge-Thierry, C., 2006. Estimating rupture scenario likelihood based on dynamic rupture simulations: the example of the segmented Middle Durance fault, southeastern France, *Geophys. J. Int.*, **165**(2), 436–446.
- Argus, D.F., Peltier, W.R. & Watkins, M.M., 1999. Glacial isostatic adjustment observed using very long baseline interferometry & satellite laser ranging geodesy, *J. Geophys. Res.*, **104**, 29 077–29 093.
- Arthaud, F. & Matte, P., 1974. Les décrochements tardi-hercyniens du SW de l'Europe. Géométrie et essai de reconstitution des conditions de la déformation, *Tectonophysics*, **25**, 139–171.
- Baize S. & Nocquet, J.M., 2006. Quantification de la déformation active autour de la faille de la Moyenne Durance par géodésie spatiale, IRSN report DEI/SARG no. 2006-053.
- Baize S., Cushing, E.M., Lemeille, F., Granier, T., Grellet, B., Carbon, D., Combes, P. & Hibsich, C., 2002. Inventaire des indices de rupture affectant le Quaternaire en relation avec les grandes structures connues, en France métropolitaine et dans les régions limitrophes, *Mém. Soc. Géol. Fr.*, **175**, 142.
- Baroux, E., 2000. Tectonique active en région à sismicité modérée: le cas de la Provence (France). Apport d'une approche pluridisciplinaire, *PhD thesis*. University of Paris-Sud, France.
- Baroux, E., Béthoux, N. & Bellier, O., 2001. Analyses of the stress field in southeastern France from earthquake focal mechanisms, *Geophys. J. Int.*, **145**, 336–348.

- Baroux, E., Pino, N.A., Valensise, G., Scotti, O. & Cushing, M.E., 2002. Source parameters of the 11 June 1909 Lambesc (Provence, southeastern France) earthquake: a reappraisal based on macroseismic, seismological and geodetic observations, *J. Geophys. Res.*, **108**(B9), doi:10.1029/2002JB002348.
- Baudrimont, A.F. & Dubois P., 1977. Un bassin Mésogéen du domaine péri-alpin: le Sud-Est de la France, *Bull. Centres Rech. Explor.-Prod. Elf Aquitaine*, **1**(1), 261–308.
- Becker, A., Blümling, P. & Müller, W.H., 1987. Recent stress field and neotectonics in the Eastern Jura Mountains, Switzerland, *Tectonophysics*, **135**(4), 277–288.
- Bellier, O., Over, S., Poisson, A. & Andrieux, J., 1997. Recent temporal stress state change and modern spatial stress field along the Northern Anatolian Fault Zone, (Turkey), *Geophys. J. Int.*, **131**, 61–86.
- Bellier, O. et al., 2004. Tectonique active et aléa sismique de la faille de Moyenne Durance. Cours et séminaires. Chaire de géodynamique. <http://www.cdf.u-3mrs.fr/~lepichon/resume`web.pdf>.
- Bendick, R. et al., 2001. The January 26, 2001 Bhuj, India earthquake, *Seism. Res. Lett.*, **3**, 328–335.
- Benedicto-Esteban, A., 1996. Modèles tectono-sédimentaires de bassins en extension et style structural de la marge passive du Golfe du Lion (Partie Nord), Sud-Est France, *PhD thesis*. Université of Montpellier II, France.
- Benedicto, A., Labaume, P., Séguret, M. & Séranne, M., 1996. Low-angle crustal ramp & basin geometry in the Gulf of Lion passive margin: Oligocene-Aquitainian Vistrenque graben, SE France, *Tectonics*, **15**(6), 1192–1212.
- Bigot-Cormier, F., Sage, F., Sosson, M., Déverchère, J., Ferrandini, M., Guennoc, P., Popoff, M. & Stéphane, J.-F., 2004. Pliocene deformation of the north-Ligurian margin (France): consequences of a south-Alpine crustal thrust. *Bulletin de la Société Géologique de France*, **175**(2), 197–211.
- Biondi, P., Lerat, O. & Philips, J., 1992. Synthèse structurale, sédimentologique et géochimique du bassin eocène-oligocène de Manosque-Forcalquier, *Report, E.N.S.P.M., IFP*.
- Bott, M.H.P., 1959. The mechanics of oblique slip-faulting, *Geol. Mag.*, **96**, 109–117.
- Cabrol, C., 1985. Etude du bassin de Manosque-Forcalquier à partir de documents sismiques, *Report E.N.S.M. Paris*.
- Calais, E., Nocquet, J.-M., Jouanne, F. & Tardy, M., 2002. Current strain regime in the Western Alps from continuous global positioning system measurements, 1996–2001, *Geology*, **30**(7), 651–654.
- Calais, E., DeMets, C. & Nocquet, J.M., 2003. Evidence for a post-3.16-Ma change in Nubia-Eurasia-North America plate motions? *Earth Planet. Sci. Lett.*, **216**, 81–92.
- Carey, E., 1979. Recherche des directions principales de contraintes associées au jeu d'une population de failles, *Rev. Geol. Dyn. Geog. Phys.*, **21**, 57–66.
- Carey, E. & Brunier, B., 1974. Analyse théorique et numérique d'un modèle mécanique élémentaire appliqué à l'étude d'une population de failles, *C. R. Acad. Sci. Paris*, **279**(Série D), 891–894.
- Carey-Gailhardis, E. & Mercier, J.-L., 1987. A numerical method for determining the state of stress using focal mechanisms of earthquake populations: application to Tibetan teleseisms and microseismicity of Southern Peru, *Earth Planet. Sci. Lett.*, **82**, 165–179.
- Carey-Gailhardis, E. & Mercier, J.-L., 1992. Regional state of stress, fault kinematics and adjustments of blocks in a fractured body of rock: application to the microseismicity of the Rhine graben, *J. Struct. Geol.*, **14**(8/9), 1007–1017.
- Champion, C., Choukroune, P. & Clauzon, G., 2000. La déformation post-Miocène en Provence occidentale, *Geodinamica Acta*, **13**, 67–85.
- Chardon, C. & Bellier, O., 2003. Geological boundary conditions of the 1909 Lambesc (Provence, France) earthquake: structure & evolution of the Trévaresse ridge anticline, *Bull. Soc. Géol. France*, **174**(5), 497–510.
- Chardon, D., Hermitte, D., Nguyen, F. & Bellier, O., 2005. First paleoseismological constraints on the strongest earthquake in France (Provence) in the twentieth century, *Geology*, **33**(11), 901–904.
- Chen, H., Chiu, J.-M., Pujol, J., Kim, K., Chen, K.-C., Huang, B.-S., Yeh, Y.-H. & Chiu, S.-C., 2006. A simple algorithm for local earthquake location using 3D V and V models: test examples in the central United States and in central eastern Taiwan, *Bull. Seism. Soc. Am.*, **96**(1), 288–305.
- Clauzon, G., 1975. Sur l'âge villafranchien du chevauchement subalpin au droit de Puimoisson (Alpes-de-Haute-Provence), *C. R. Acad. Sci. Paris*, **280**, 2433–2436.
- Clauzon, G., 1984. Évolution d'une montagne provençale et de son piémont: l'exemple du Lubéron, in *Montagnes et Piémonts*, *R.G.P.S.O.*, Toulouse.
- Combes P., 1984. La tectonique récente de la Provence occidentale: microtectonique, caractéristiques dynamiques et cinématiques. Méthodologie de zonation tectonique et relations avec la sismicité, *PhD thesis*. University of L. Pasteur of Strasbourg, France.
- Crone, A.J., 1998. Defining the southwestern end of the Blytheville Arch, northeastern Arkansas: delimiting a seismic source zone in the New Madrid region, *Seismol. Res. Lett.*, **69**(4), 350–358.
- Crone, A.J., McKeown, F., Harding, S., Hamilton, R., Russ, D. & Zoback, M., 1985. Structure of the New Madrid seismic source zone in southeastern Missouri and northeastern Arkansas, *Geology*, **13**(8), 547–550.
- Cushing, M., Volant, P., Bellier, O., Sébrier, M., Baroux, E., Grellet, B., Combes, P. & Rosique, T., 1997. A Multidisciplinary Experiment to Characterize an Active Fault System in Moderate Seismic Activity Area: The Example of the Durance Fault (South East France), EGS XXII General Assembly, Vienna, Blackwell, Oxford.
- Cushing, M., Bellier, O., Volant, P., Aochi, H., Baize, S. & Berge-Thierry, C., 2004. Recent findings integrated in seismic hazard assessment: the case study of the Durance fault, in *Committee on the Safety of Nuclear Installations CSNI Workshop on "Seismic Input Motions, Incorporating Recent Geological Studies"* Tsukuba, Japan.
- Debrand-Passard, S., Courbouleix, S. & Lienhardt, M.J., 1984. Synthèse géologique du Sud-Est de la France, *Mém. BRGM Orléans*, Vol. **125**, France.
- DeMets, C., Gordon, R.G., Argus, D.F. & Stein, S., 1990. Current plate motions, *Geophys. J. Int.*, **101**, 425–478.
- DeMets, C., Gordon, R.G., Argus, D.F. & Stein, S., 1994. Effect of recent revisions of the geomagnetic reversal time scale on estimates of current plate motions, *Geophys. Res. Lett.*, **21**, 2191–2194.
- Dubois, P. & Curnelle, R., 1978. Résultats apportés par le forage des Mées n° 1 sur le plateau de Valensole (Alpes de Haute-Provence), *Comptes Rendus Som. Soc. Géol. France*, **4**, 181–184.
- Dutour, A., Philip, H., Jaurand, E. & Combes, P., 2002. Mise en évidence de déformations en faille inverse avec ruptures de surface cosismiques dans des dépôts colluviaux würmiens du versant nord du mont Ventoux (Provence occidentale, France), *C. R. Geosci.*, **334**, 849–856.
- Ferhat, G., Feigl, K.L., Ritz, J.-F. & Souriau, A., 1998. Geodetic measurement of tectonic deformation in the southern Alps & Provence, France, 1947–1994, *Earth Planet. Sci. Lett.*, **159**, 35–46.
- Gephart, J.W. & Forsyth, D.W., 1984. An improved for determining the regional stress tensor using earthquake focal mechanism data: an application to the San Fernando earthquake sequence, *J. geophys. Res.*, **89**, 9305–9320.
- Ghafiri, A., 1995. Paléosismicité de failles actives en contexte de sismicité modérée: application à l'évaluation de l'aléa sismique dans le Sud-Est de la France, *PhD thesis*. University of Paris-Sud, France.
- Ghafiri, A., Sauret, B., Rosique, T., Blès, J.L. & Sébrier, M., 1993. Mise en évidence d'un paléoséisme sur la faille de la Moyenne Durance, *Géol. Alpine Série spéciale*. Résumés de colloque, **2**, 24–25.
- Guignard, P., Bellier, O. & Chardon, D., 2005. Géométrie et cinématique post-oligocène des Failles d'Aix et de la Moyenne Durance (Provence, France), *C.R. Géoscience, Acad. Sc. Paris*, **337**(3), 483–573.
- Guignard, P., 2002. Géométrie et cinématique de la terminaison méridionale du segment central de la Faille de la Moyenne Durance (Zone de Beaumont-de-Pertuis et Mirabeau), *Mémoire de DEA Géosciences de l'Environnement*, University of Aix-Marseille III, France.
- Hanks, T.C. & Kanamori, H., 1979. A moment-magnitude scale, *J. geophys. Res.*, **84**, 2348–2350.

- Hippolyte, J.C. & Dumont, T., 2000. Identification of Quaternary thrusts, folds & faults in a low seismicity area: examples in the Southern Alps (France), *Terra Nova*, **12**, 156–162.
- Lacassin, R., Tapponnier, P., Meyer, B. & Armijo, R., 2001. Was the Trévasse thrust the source of the 1909 Lambesc (Provence, France) earthquake? Historical & geomorphic evidence, *C. R. Acad. Sci.*, **333**, 571–581.
- Lambert, I., Levret-Albaret, A., Cushing, M. & Durouchoux, C., 1996. Mille Ans de Séismes en France, *Ouest Edn.*, Paris.
- Larroque, C., et al. 2001. Active & recent deformation at the Southern Alps – Ligurian basin junction, *Netherlands J. Geosci./Geol. en Mijnbouw*, **80**(3–4), 255–272.
- Laurent, O., Stephan, J.-F. & Popoff, M., 2000. Modalités de la structuration miocène de la branche sud de l'arc de Castellane (chaînes subalpines méridionales), *Géol. France*, **3**, 33–65
- Le Pichon, X., 2004. La déformation active du Sud-Est de la France, Conference. (http://www.cdf.u-3mrs.fr/~lepichon/resume_web.pdf).
- Lebatard, A.E., 2003. Activité tectonique et alea sismique de la terminaison septentrionale de la faille de la Moyenne Durance et ses relations avec la nappe de Digne, *Mémoire de DEA Géosciences de l'Environnement*, University of Aix-Marseille III, France.
- Leturmy, P., Dumont, T., Van Der Beek, P. & Champagnac, J.D., 1999. Recent deformation of the Valensole plateau (SE France): Alpine thrust propagation versus Ligurian regional stress? *Abstracts of the 4th Workshop on Alpine Geological Studies, Tübingen 21–24 Sept.* <http://homepages.uni-tuebingen.de/alpshp/TGAvol-030.html>
- Levret, A., Backe, J.C. & Cushing, M., 1994. Atlas of macroseismic maps for French earthquakes with their principal characteristics, *Natural Hazards*, **10**(1–2), 19–46.
- Lickorish, W.H. & Ford, M., 1998. Sequential restoration of the external Alpine Digne thrust system, SE France, constrained by kinematic data & synorogenic sediments, *Geol. Soc. Special Publ.*, **134**, 189–211
- Lickorish, W.H., Ford, M., Burgisser, J. & Cobbold, P.R., 2002. Arcuate thrust systems in sandbox experiments: a comparison to the external arcs of the Western Alps, *Bull. Geol. Soc. Am.*, **114**(9), 1089–1107.
- Lomax, A., 2005. A reanalysis of the hypocentral location & related observations for the great 1906 California earthquake, *Bull. Seism. Soc. Am.*, **91**, 861–877.
- Lomax, A. & Curtis, A., 2001. Fast, probabilistic earthquake location in 3D models using Oct-Tree Importance sampling, *Geophys. Res. Abstr.*, **3**.
- Lomax, A., Virieux, J., Volant, P. & Berge, C., 2000. Probabilistic earthquake location in 3D & layered models: introduction of a Metropolis-Gibbs method & comparison with linear locations, in *Advances in Seismic Event Location*, pp. 101–134, eds. Thurber, C.H. & Rabinowitz, N., Kluwer, Amsterdam.
- Meyer, B., Sébrier, M. & Dimitrov, D., 2007. Rare destructive earthquakes in Europe: the 1904 Bulgaria event case, *Earth Planet. Sci. Lett.*, **253**(3–4), 485–496.
- Mercier, J.L., Carey-Gailhardis, E. & Sébrier, M., 1991. Paleostress determinations from fault kinematics: application to the neotectonics of the Himalaya-Tibet and the Central Andes, *Phil. Trans. R. Soc. Lond., A*, **337**, 41–52.
- Nechtschein, S., 2003. Calcul d'une magnitude de moment M_w pour les séismes enregistrés par le réseau de la Durance. *IRS report DEI/SARG no. 2003-01*.
- Nguyen, F.H., 2005. Near-surface Geophysical Imaging & Detection of Slow Active faults, *PhD thesis*. Faculty of Applied Sciences, Liège University, Belgium.
- Nicolas, M., Sautoire, J.P. & Delpech, P.Y., 1990. Intraplate seismicity: new seismotectonic data in western Europe, *Tectonophysics*, **179**, 27–53.
- Nocquet, J.M., 2002. Mesure de la déformation crustale en Europe occidentale par géodésie spatiale, *PhD thesis*. Nice University, Sophia Antipolis, France.
- Nocquet, J.M. & Calais, E., 2004. Geodetic Measurements of Crustal Deformation in the Western Mediterranean & Europe, *Pure Appl. Geophys.*, **161**(3), 661–681.
- Quenet, G., Baumont, D., Scotti, O. & Levret, A., 2004. The August 14th, 1708 Manosque, France earthquake: new constraints on the damage area from in-depth historical studies, *Ann. geophys.*, **47**(2/3).
- Reasenber, P.A. & Oppenheimer, D., 1985. FPFIT, FPLOT, & FPPAGE: Fortran computer programs for calculating & displaying earthquake fault-plane solutions, *U.S. Geol. Surv. Open-File Rep.*, 85–739.
- Roure, F. & Colletta, B., 1996. Cenozoic inversion structures in the foreland of the Pyrenees & Alps, in *Peri-Tethys Memoir 2: Structure & Prospects of Alpine Basins & Forelands*, pp. 173–209, eds. Ziegler, P.A. & Horvath, F., *Mém. Mus. Nat. Hist. Not.*, **170**. Paris ISBN:2-85653-507-0.
- Roure, F., Brun, J.P., Colletta, B. & Van Den Driessche, J., 1992. Geometry & kinematics of extensional structures in the Alpine Foreland Basin of southeastern France, *J. Struct. Geol.*, **14**(5), 503–519.
- Rousset, C., 1978. De l'importance régionale de la faille d'Aix-en-Provence, *C. R. Acad. Sci. Paris*, **286**, 89–191.
- Schwartz, D.P. & Coppersmith, K.J., 1984. Fault behavior and characteristic earthquakes: examples from the Wasatch and San Andreas fault zones, *J. Geophys. Res.*, **89**, 5681–5698.
- Scotti, O., Baumont, D., Quenet, G. & Levret, A., 2004. The French macroseismic database SISFRANCE – objectives, results and perspectives, *Ann. geophys.*, **47**(2–3), 571–581.
- Sébrier, M., Ghafiri, A. & Blès, J.L., 1997. Paleoseismicity in France: fault trench studies in a region of moderate seismicity, *J. Geodyn.*, **24**, 207–217.
- Sébrier, M., Siame, L., Bellier, O. & Chardon, D., 2004. Slow active faults in compressional settings. Seismotectonic model for Provence SE France. Slow active faults in Europe (s.a.f.e.). assessing fundamental input for seismic risk in regions of low seismicity, Project EVG1–2000-22005 (contract EVG1-CT-2000-00023), 97–127.
- Siame, L. et al., 2004. Local erosion rates versus active tectonics: cosmic ray exposure modelling in Provence (south-east France), *Earth Planet. Sci. Lett.*, **220**(3–4), 345–364.
- Terrier, M., 1991. Néotectonique de la Provence occidentale (France): Vers une analyse multicritère de déformation récente. Application à la Classification des structures sismogènes, *PhD thesis*. University of Provence-Marseille, France.
- Tuttle, M.P., Lafferty, R.H., Guccione, M.J., Schweig, E.S., Lopinot, N., Cande, R.F., Dyer-Williams, K. & Haynes, M., 2002. The earthquake potential of the New Madrid Seismic Zone, *Bull. Seism. Soc. Am.*, **6**, 2080–2089.
- Vanneste, K. et al., 2006. Paleoseismologic investigation of the fault rupture of the 14 April 1928 Chirpan earthquake (M 6.8), southern Bulgaria, *J. geophys. Res. B: Solid Earth*, **111**(1), art. no. B01303.
- Vasseur, G., Etchecopar, A. & Philip, H., 1983. Stress state inferred from multiple focal mechanisms, *Ann. geophys.*, **1**, 291–298.
- Villéger M., 1984. Evolution tectonique du panneau de couverture Nord-Provençale (Mont-Ventoux, Lubéron, Moyenne Durance), *PhD thesis*. University of Paris-Sud, France.
- Villéger, M. & Andrieux, J., 1987. Phases tectoniques post-éocènes et structuration polyphasée du panneau de couverture nord provençal (Alpes externes méridionales), *Bull. Soc. Géol. Fr.*, **8**(3), 147–156.
- Volant, Ph., Berge-Thierry, C., Dervin, P., Cushing, M., Mohammadiou, G. & Mathieu, F., 2000. The South Eastern Durance fault permanent network: preliminary results, *J. Seismol.*, **4**, 175–189.
- Volant, P., Lomax, A., Nechtschein, S., Cushing, M., Ait-Ettajer, T., Berge-Thierry, C. & Dervin, P., 2003. Localisation 3D et calcul de magnitude pour les évènements du réseau Durance, *6ème colloque National de l'Association Française de Génie Parasismique, Ecole Polytechnique, Palaiseau (France)*, 1–3 Juillet. **1**, 21–32.
- Wells, D. & Coppersmith, K.J., 1994. New empirical relationships among magnitude, rupture length, rupture area & surface displacement, *Bull. Seism. Soc. Am.*, **84**(4), 974–1002.
- Wesnousky, S.G., 1986. Earthquakes, quaternary faults & seismic hazard in California, *J. geophys. Res.*, **91**, 12 587–12 631.

APPENDIX A: SEGMENTATION DESCRIPTION OF THE MDF AND ASSOCIATED ACTIVE FAULTS

No.	Name – length – strike	Main observations and interpretation
MDF Segment 1	Venelles-Meyrargues – 8 km – N025°E	Vertical offset of a roman aqueduct pointed out by leveling. Post Oligocene sinistral strike-slip fault plane east of Meyrargue town (Guignard <i>et al.</i> 2005).
Segment 2	Loubière-Mirabeau – 8 km – N060°E	Connected to the South with Trevaresse Fault (Chardon & Bellier, 2003) Boundary between Oligocene beds and cretaceous limestones The northern part of this segment does not seem to reach segment 3. Segment 2 is relayed by the “horse tail” termination of segment 3 (Guignard <i>et al.</i> 2005). The whole segment is poorly mapped.
Segment 3	Mirabeau-Manosque. – 18 km – N045°E	Geological contact between Mesozoic series (W) and folded Miocene series (E) located by surface projection of faults observed on seismic sections. Connected to the south to a horse tail termination which could be extended to the Costes thrust through the Durance Valley to the West. Well constrained mapping in the southernmost part
Segment 4	Manosque-Villeneuve East – 9 km – N030°E	Inferred from seismic section interpretation and morphological analysis. The SE-facing slope between lower the intermediate terraces may be considered as an escarpment partly formed by a fault (Siame <i>et al.</i> 2004).
Segment 5	Villeneuve-Peyruis – 15 km – N020°E	In the south near La Brillanne town, an outcrop located on the slope lying along the motorway, shows a fault affecting rissian quaternary terrace (Terrier, 1991). It may not be autochthonous, and probably corresponds to a landslide along this slope (Baroux 2000). Further north, a steep slope underlines the fault trace where the Durance river reaches the valley edge. This may indicate a recent activity of this segment.
Segment 6	Peyruis-Chateau-Arnoux 12 km – N040°E	This fault segment does not exhibit any outcrop evidence of faulting and is probably blind. However seismic section 71D8 crosscuts the fault and shows this segment at depth.
Segment 7	Chateau-Arnoux-Valavoire 14 km – N020°E	No direct evidence of surface faulting can be pointed out from this segment. Only local minor faults, “en echelon” shape folding and morphological anomalies (Lebatard, 2003) can be observed. From those features, the MDFZ is supposed to affect the sedimentary cover at depth (blind fault).
Segments 8	Manosque-Villeneuve West – 11 km – N050°E	Its projection to surface combined with some structural observations such as the rapid transition between weakly dipping and strong dipping or overturned Miocene beds locate a reversed listric fault crossing the Valveranne and the Fontamauri valley. On seismic section VL850, the westernmost discontinuity probably corresponds to that feature. This fault is anchored in Triassic layers
Segment 9:	ST Paul-Ste Tulle – 8 km – N020°E	This north-trending fault segment is only deduced from indirect observations: (1) the left-lateral “en baionnette” trace of the talwegs and (2) the aligned anomalies in the longitudinal profiles across homogeneous conglomerates. (Guignard <i>et al.</i> 2005). The microseismicity detected by the Durance network strengthens the presence of this segment.
Other fault systems coupled with the MDF	S 10: Pierreverit – Bastide des Jourdans East Luberon fault – 9 km and S 11: Luberon south verging fault — 17 km	These segments are probably blind locally (Champion <i>et al.</i> 2000). They have been assumed from geological maps, that is, fault trace and/or rapid dipping change on the frontal limb of dissymmetric Manosque-Luberon anticline and from surface projection of faults identified on seismic sections. These features are anchored within Triassic ductile levels. N 080
	S11-S12: Trevaresse Fault 7 and 9 km segments	These segments are responsible for 1909 $M_w \sim 6.0$ earthquake. This feature has been fully described by, Lacassin <i>et al.</i> (2001), Chardon & Bellier (2003) and palaeoseismic evidence are documented in Chardon <i>et al.</i> 2005.

APPENDIX B: BEST LOCATED EVENTS BY THE DURANCE NETWORK BETWEEN 1999 AND 2006

Table B1. N. a. t. corresponds to number of arrival times. Az1, Dip1, Se1, Az2, Dip2, Se2, Se3, indicate azimuths, dips and half-lengths of the axes of the 68 per cent confidence ellipsoid approximation to the location probability density function. FMS is the focal solution number used in the Appendix C table.

Date dd/mm/yyyy	Long. °E (d.ddd)	Lat °E (d.ddd)	Depth (km)	M_L	N. a. t.	rms (s)	Az1 (°)	Dip1 (°)	Se1 (km)	Az2 (°)	Dip2 (°)	Se2 (km)	Se3 (km)	FMS number
03/01/1999 21:26	5.661	43.710	-2.4	0.56	6	0.06	351	-2	0.3	82	-25	0.7	1.6	
02/06/1999 02:18	5.880	44.006	-6.8	1.24	8	0.10	97	5	0.3	187	7	0.9	1.8	
29/09/1999 04:40	5.933	43.701	-8.5	2.07	17	0.09	211	-3	0.2	121	3	0.4	0.7	1
12/12/1999 10:46	5.704	43.835	-0.9	2.25	20	0.08	198	0	0.2	108	10	0.3	1.4	2
30/06/2000 09:44	5.815	43.635	-0.7	1.35	11	0.10	193	-3	0.2	105	23	0.3	0.5	
21/07/2000 17:47	5.572	43.694	0.1	0.99	8	0.12	221	-1	0.3	131	2	0.6	1.3	
08/08/2000 20:13	5.824	43.634	-1.3	0.94	8	0.06	189	0	0.2	100	23	0.4	0.7	
25/08/2000 20:34	5.783	43.853	-2.7	1.62	16	0.29	195	10	0.2	91	55	0.2	0.3	3
18/09/2000 21:09	5.728	43.914	-8.8	1.51	12	0.08	196	22	0.3	104	5	0.6	0.8	4
18/09/2000 22:33	5.726	43.916	-8.1	1.22	8	0.04	23	-15	0.4	292	-1	0.6	0.9	
21/10/2000 13:14	5.836	43.639	-1.5	0.89	10	0.10	182	-8	0.3	93	5	0.4	0.8	
17/01/2001 08:17	5.873	44.032	-3.9	1.36	8	0.12	82	11	0.5	173	2	0.9	1.7	
27/01/2001 02:56	5.685	43.715	-2.5	2.46	20	0.05	200	-5	0.2	111	12	0.2	0.5	5
28/01/2001 07:55	5.804	43.659	0.5	1.32	13	0.13	178	-7	0.2	89	7	0.3	1.3	
19/02/2001 18:56	5.769	43.829	-3.3	1.29	14	0.08	193	-1	0.2	103	11	0.3	1.2	6
19/03/2001 11:19	5.645	43.731	0.5	1.67	7	0.19	160	-1	0.3	71	5	0.6	1.4	
03/04/2001 21:43	5.600	43.668	-2.3	1.33	12	0.17	231	-23	0.2	327	-11	0.3	0.9	7
18/05/2001 12:34	5.729	43.727	-1.9	2.13	20	0.06	230	-33	0.2	329	-12	0.2	0.3	8
19/05/2001 07:30	5.733	43.724	-1.7	2.80	19	0.13	212	-7	0.2	122	0	0.2	0.9	9
19/05/2001 21:10	5.726	43.731	-2.1	2.25	20	0.05	215	-9	0.2	128	17	0.2	0.6	10
31/05/2001 08:18	5.720	43.729	-2.3	1.35	12	0.09	178	-2	0.2	88	13	0.3	1.0	11
26/07/2001 10:40	5.680	43.693	-2.8	1.75	15	0.05	192	-4	0.2	103	11	0.3	0.8	12
26/07/2001 10:42	5.683	43.694	-2.6	1.54	14	0.06	190	-5	0.2	101	10	0.3	0.7	13
12/08/2001 21:42	5.820	43.637	-1.5	1.35	11	0.04	83	73	0.2	56	-14	0.3	0.6	14
30/08/2001 03:53	5.678	43.688	-1.3	1.39	12	0.15	347	-1	0.2	77	0	0.3	1.4	
16/09/2001 04:22	5.690	43.739	-2.9	2.05	19	0.10	212	-9	0.2	125	18	0.2	0.4	15
10/11/2001 20:39	5.697	43.729	-1.6	0.80	8	0.05	165	1	0.3	75	15	0.4	1.3	
08/02/2002 22:08	5.675	43.744	-0.1	0.49	6	0.02	326	4	0.3	62	57	0.9	1.7	
13/04/2002 11:00	5.830	43.639	-1.7	1.31	14	0.07	14	34	0.2	41	-52	0.2	0.3	16
28/04/2002 01:28	5.681	43.670	-0.8	0.95	6	0.02	44	2	0.3	134	-2	0.5	1.9	
02/06/2002 07:06	5.957	43.837	-7.8	1.25	11	0.10	226	8	0.3	137	-12	0.5	0.9	17
13/06/2002 17:55	5.678	43.676	-4.5	1.42	19	0.10	204	-8	0.2	115	1	0.3	0.7	18
23/06/2002 11:04	5.639	43.635	-3.7	1.39	11	0.11	67	8	0.3	155	-14	0.4	0.7	19
10/07/2002 01:14	5.633	43.636	-6.2	1.99	14	0.10	245	-16	0.3	332	10	0.3	0.9	20
07/08/2002 02:26	5.665	43.715	-2.6	1.77	15	0.12	170	7	0.2	75	34	0.3	0.6	21
13/02/2003 00:19	5.833	43.666	0.5	0.90	5	0.01	318	-3	0.5	226	-25	1.1	1.2	
13/08/2003 00:27	5.782	43.789	-4.4	1.31	12	0.09	193	-3	0.2	103	0	0.3	1.4	22
06/10/2003 16:39	6.037	43.776	-9.3	1.33	10	0.10	211	10	0.3	106	55	0.8	1.5	
02/02/2004 18:25	5.637	43.811	-3.5	1.58	15	0.08	195	-2	0.2	106	10	0.4	0.7	23
09/02/2004 03:58	5.813	43.640	-1.3	0.94	7	0.11	51	4	0.3	143	25	0.8	1.2	
04/03/2004 01:07	5.696	43.719	-1.1	0.67	7	0.04	143	7	0.3	52	5	0.5	1.1	
23/04/2004 12:27	5.622	43.752	-2.9	1.31	11	0.07	169	-2	0.3	81	33	0.5	0.7	
25/06/2004 12:07	5.717	43.701	-2.9	1.58	14	0.08	180	-5	0.2	90	2	0.3	0.8	24
03/08/2004 01:20	5.748	43.826	-3.5	1.30	8	0.33	219	2	0.3	129	6	0.4	1.2	
04/09/2004 15:23	6.094	43.736	-13.7	1.61	11	0.08	200	6	0.3	106	33	0.8	1.4	
04/09/2004 20:13	5.859	43.917	-2.5	1.86	16	0.07	91	15	0.2	185	13	0.3	1.1	25
29/10/2004 08:52	5.818	43.659	-1.7	1.72	15	0.07	5	56	0.2	33	-30	0.3	0.3	
31/10/2004 10:44	5.664	43.907	-10.5	1.14	6	0.05	221	10	0.5	125	31	0.9	1.3	
16/11/2004 04:30	5.863	43.943	-2.9	1.18	11	0.04	280	-8	0.3	10	-3	0.3	1.5	
28/01/2005 03:50	5.575	43.588	-5.7	1.73	11	0.18	291	-16	0.4	14	20	0.6	1.2	26
08/03/2005 21:16	5.785	43.867	-0.3	0.56	5	0.02	275	27	0.4	203	-31	1.1	1.5	
20/03/2005 14:13	5.844	43.903	-0.2	1.57	20	0.11	304	-4	0.1	34	-5	0.2	0.8	27
02/04/2005 12:59	5.816	43.639	-1.1	1.18	8	0.12	176	-4	0.2	86	4	0.5	1.1	
01/07/2005 09:50	5.834	43.641	0.3	1.23	10	0.10	199	-9	0.3	109	1	0.3	0.8	
23/08/2005 23:31	5.691	43.740	-2.9	2.03	11	0.12	232	-22	0.2	337	-31	0.3	0.4	
04/11/2005 04:21	5.770	43.866	0.0	0.61	8	0.04	233	4	0.3	144	-15	0.4	1.5	
09/11/2005 20:17	5.696	43.760	-3.3	1.75	13	0.11	175	7	0.2	79	40	0.3	0.7	
02/02/2006 18:05	5.664	43.708	-2.2	1.1	7	0.05	209	4	0.3	118	4	0.4	1.1	
11/02/2006 20:26	5.602	43.608	-8.7	2.0	17	0.21	277	-17	0.3	0	20	0.4	0.8	

APPENDIX C: RETAINED FOCAL SOLUTIONS

Ev. N°	Sol. Numb.	Date-time yyymmddhhmm	Depth km	M_L	STRD	Nodal plane A			Nodal plane B			P axis		T axis	
						Az.	Dip	Rake	Az.	Dip	Rake	Az.	Pl.	Az.	Pl.
1	1	199909290440	8.51	2.1	0.83	315	81	-137	217	48	-12	186	36	79	21
1	2	199909290440	8.51	2.1	0.68	270	7	57	123	84	94	210	39	37	51
2	1	199912121046	0.91	2.2	0.69	101	56	117	239	42	56	172	7	65	67
2	2	199912121046	0.91	2.2	0.25	329	10	177	62	89	80	162	44	323	45
3	1	200008252034	2.70	1.6	0.73	290	69	-137	182	50	-28	153	45	52	11
3	2	200008252034	2.70	1.6	0.61	93	38	-177	1	88	-52	303	35	60	32
4	1	200009182109	8.85	1.5	0.69	138	57	160	239	73	35	5	11	103	36
4	2	200009182109	8.85	1.5	0.56	161	81	141	258	52	12	215	19	112	33
4	3	200009182109	8.85	1.5	0.49	201	7	-101	32	83	-89	304	52	121	38
5	1	200101270256	2.55	2.5	0.83	177	61	-17	275	75	-150	140	32	44	9
6	1	200102191856	3.31	1.3	0.40	352	71	-57	109	38	-148	302	52	58	19
6	2	200102191856	3.31	1.3	0.73	198	62	-17	296	75	-151	160	31	65	9
6	3	200102191856	3.31	1.3	0.54	299	32	163	44	81	59	158	29	283	45
7	1	200104032143	2.33	1.3	0.74	248	88	-23	339	67	-178	202	18	296	15
8	1	200105181234	1.90	2.1	0.64	111	49	-118	330	48	-62	312	69	220	0
9	1	200105190730	1.70	2.8	0.62	112	61	-143	2	58	-35	329	46	236	2
9	2	200105190730	1.70	2.8	0.47	334	40	-78	138	51	-100	1	80	236	6
9	3	200105190730	1.70	2.8	0.44	225	65	78	72	28	114	324	19	112	68
10	1	200105192110	2.14	2.2	0.76	94	81	177	184	87	9	319	4	50	8
10	2	200105192110	2.14	2.2	0.79	185	81	23	91	67	170	316	9	50	23
11	1	200105310818	2.30	1.4	0.66	75	21	103	241	70	85	335	24	143	65
11	2	200105310818	2.30	1.4	0.62	114	80	-143	17	54	-12	342	33	240	17
11	3	200105310818	2.30	1.4	0.64	116	81	-157	22	67	-10	342	23	247	9
12	1	200107261040	2.75	1.7	0.35	142	62	-101	344	30	-70	28	71	240	16
13	1	200107261042	2.61	1.5	0.80	177	60	-17	276	75	-149	140	32	44	10
13	2	200107261042	2.61	1.5	0.51	268	29	-177	175	89	-61	112	40	241	37
13	3	200107261042	2.61	1.5	0.55	255	69	163	351	74	22	122	3	215	27
14	1	200108122142	1.51	1.3	0.69	281	87	37	189	53	176	49	23	151	28
15	1	200109160422	2.91	2.1	0.71	232	62	17	134	75	151	186	9	90	31
15	2	200109160422	2.91	2.1	0.28	347	18	-179	256	90	-72	184	43	329	42
15	3	200109160422	2.91	2.1	0.58	262	42	57	123	56	116	195	7	87	67
16	1	200204131100	1.69	1.3	0.71	48	81	-177	318	87	-9	273	8	3	4
16	2	200204131100	1.69	1.3	0.83	153	80	63	44	29	159	265	30	34	48
17	1	200206020706	7.83	1.3	0.67	57	88	-2	147	88	-178	12	3	283	0
18	1	200206131755	4.46	1.4	0.43	176	25	-97	4	65	-87	281	70	91	20
19	1	200206231104	3.73	1.4	0.76	218	87	-21	309	69	-177	172	17	265	12
20	1	200207100114	6.22	2.0	0.75	47	87	20	316	70	177	180	12	274	16
20	2	200207100114	6.22	2.0	0.44	62	72	97	220	19	69	146	27	343	62
21	1	200208070226	2.56	1.8	0.44	9	90	-57	99	33	-180	308	36	70	36
21	2	200208070226	2.56	1.8	0.46	235	41	43	110	63	122	177	13	66	58
22	1	200308130027	4.39	1.3	0.78	215	84	-17	307	73	-174	170	16	262	8
23	1	200402021825	3.48	1.6	0.89	109	45	102	272	46	78	11	1	105	82
23	2	200402021825	3.48	1.6	0.75	325	78	177	56	87	12	190	6	281	11
24	1	200406251207	2.86	1.6	0.64	7	43	-98	198	48	-83	170	84	283	2
24	2	200406251207	2.86	1.6	0.42	268	24	-121	121	70	-77	52	63	202	24
25	1	200409042013	2.54	1.9	0.76	248	25	-63	39	68	-102	289	65	138	22
26	1	200501280350	5.75	1.7	0.29	190	42	43	65	63	123	132	12	23	58
27	1	200503201413	0.24	1.6	0.87	210	67	-17	307	74	-156	170	28	77	5
27	2	200503201413	0.24	1.6	0.61	96	80	83	311	12	125	192	35	358	54
27	3	200503201413	0.24	1.6	0.67	262	15	77	95	75	93	183	30	10	59